AFRL-ML-WP-TP-2007-455

ON THE BIFURCATION OF THE THERMO-ELASTIC DEFORMATION OF AN ASYMMETRIC PLATE (PREPRINT)

George Jefferson
Triplicane Parthasarathy

MAY 2007

Approved for public release; distribution unlimited.

STINFO COPY

This work was funded in whole or in part by Department of the Air Force contract FA8650-04-D-5233. The U.S. Government has for itself and others acting on its behalf an unlimited, paid-up, nonexclusive, irrevocable worldwide license to use, modify, reproduce, release, perform, display, or disclose the work by or on behalf of the U.S. Government.

MATERIALS AND MANUFACTURING DIRECTORATE
AIR FORCE RESEARCH LABORATORY
AIR FORCE MATERIEL COMMAND
WRIGHT-PATTERSON AIR FORCE BASE, OH 45433-7750

REPORT DOCUMENTATION PAGE

Form Approved
OMB No. 0704-0188

1. REPORT DATE *(DD-MM-YY)*	2. REPORT TYPE	3. DATES COVERED *(From - To)*
May 2007	Journal Article Preprint	

4. TITLE AND SUBTITLE
ON THE BIFURCATION OF THE THERMO-ELASTIC DEFORMATION OF AN ASYMMETRIC PLATE (PREPRINT)

5a. CONTRACT NUMBER
FA8650-04-D-5233

5b. GRANT NUMBER

5c. PROGRAM ELEMENT NUMBER
62102F

6. AUTHOR(S)
George Jefferson
Triplicane Parthasarathy

5d. PROJECT NUMBER
2311

5e. TASK NUMBER
00

5f. WORK UNIT NUMBER
02

7. PERFORMING ORGANIZATION NAME(S) AND ADDRESS(ES)
UES Inc.
4401 Dayton-Xenia Road
Dayton, OH 45432-1894

8. PERFORMING ORGANIZATION REPORT NUMBER

9. SPONSORING/MONITORING AGENCY NAME(S) AND ADDRESS(ES)
Materials and Manufacturing Directorate
Air Force Research Laboratory
Air Force Materiel Command
Wright-Patterson AFB, OH 45433-7750

10. SPONSORING/MONITORING AGENCY ACRONYM(S)
AFRL-ML-WP

11. SPONSORING/MONITORING AGENCY REPORT NUMBER(S)
AFRL-ML-WP-TP-2007-455

12. DISTRIBUTION/AVAILABILITY STATEMENT
Approved for public release; distribution unlimited.

13. SUPPLEMENTARY NOTES
Journal article submitted to the International Journal of Engineering Science. This work was funded in whole or in part by Department of the Air Force contract FA8650-04-D-5233. The U.S. Government has for itself and others acting on its behalf an unlimited, paid-up, nonexclusive, irrevocable worldwide license to use, modify, reproduce, release, perform, display, or disclose the work by or on behalf of the U.S. Government.

PAO Case Number: AFRL/WS 07-1056, 27 Apr 2007. Paper contains color content.

14. ABSTRACT
The deformation of a thin flat elastic plate typically exhibits classic elastic bifurcation behavior when subjected to a through-thickness-graded thermal, or other inelastic, strain. For small strain there is a unique solution to the governing equations, while for larger strain multiple equilibrium solutions exist. Physically, the plate will initially deform to a particular shape or mode and when a critical strain is reached the mode of deformation will snap to a secondary form. This problem has been examined numerous times in the literature. However, in the special case of square symmetry, in both plate shape and materials properties, additional equilibrium deformation modes become available which are not predicted by the existing calculations. In this paper, analytic solutions are presented for these additional bifurcation modes, and the stability of these solutions was evaluated numerically. It is shown that for certain plate materials and geometry the special-case modes occur at a significantly lower strain than predicted by existing analyses. The predictions are verified by comparison with a finite element simulation.

15. SUBJECT TERMS
Bifurcation, Thermo-elastic deformation, asymmetric plate

16. SECURITY CLASSIFICATION OF:			17. LIMITATION OF ABSTRACT:	18. NUMBER OF PAGES	19a. NAME OF RESPONSIBLE PERSON (Monitor)
a. REPORT	b. ABSTRACT	c. THIS PAGE			Randall S. Hay
Unclassified	Unclassified	Unclassified	SAR	30	19b. TELEPHONE NUMBER *(Include Area Code)* N/A

Standard Form 298 (Rev. 8-98)
Prescribed by ANSI Std. Z39-18

On the bifurcation of the thermo-elastic deformation of an asymmetric plate.

George Jefferson, Triplicane A. Parthasarathy
UES, Inc., Dayton OH 45432

Abstract

The deformation of a thin flat elastic plate typically exhibits classic elastic bifurcation behavior when subjected to a through-thickness-graded thermal, or other inelastic, strain. For small strain there is a unique solution to the governing equations, while for larger strain multiple equilibrium solutions exist. Physically, the plate will initially deform to a particular shape or mode and when a critical strain is reached the mode of deformation will snap to a secondary form. This problem has been examined numerous times in the literature. However, in the special case of square symmetry, in both plate shape and materials properties, additional equilibrium deformation modes become available which are not predicted by the existing calculations. In this paper, analytic solutions are presented for these additional bifurcation modes, and the stability of these solutions are evaluated numerically. It is shown that for certain plate materials and geometry the special-case modes occur at a significantly lower strain than predicted by existing analyses. The predictions are verified by comparison with a finite element simulation.

Introduction

When a nominally flat elastic plate is subject to a through-thickness-graded intrinsic stressing the plate will develop a curvature or warp. Examples of such intrinsic stressing can be the result of a grading of the thermal expansion of the material combined with a uniform temperature change, grading of the temperature itself over a uniform material, residual stressing resulting from deposition or other materials processing effects, hygroscopic effects and so on. As the motivation for this work was an experimental observation of a thermal-expansion-graded plate we will use the term thermal strain interchangeably with inelastic or intrinsic strain.

Typically, for small imposed thermal strain there is a unique deformation mode, but for sufficiently large strain multiple equilibrium solutions become available. At the critical point where multiple solutions become available the small deformation 'primary' solution looses stability and the deformed shape of the plate will transition to one of the secondary solutions, i.e. a stable-symmetric bifurcation is observed (Thompson and Hunt, 1973). For example, in the case of in-plane isotropy, in both the elastic response and intrinsic driving stress, the initial deformation shape is bowl-like, i.e. a locally spherical, shape develops, irrespective of the shape and dimensions of the plate. For larger stressing however the deflection is approximately ellipsoidal and the plate has a cylindrical appearance when the ellipse aspect ratio is large. In this paper for we will refer to this as a cylindrical deformation. The transition point from spherical to cylindrical is dependant on the dimensions of the plate. The orientation of the axis of

the cylindrical deformation is determined by the shape of the plate, as well as the constituent response, i.e. for isotropic materials, the orientation is arbitrary for a circular plate and oriented parallel to one edge for a rectangular plate. Figure 1 shows the various deformation shapes schematically.

This problem has been extensively examined in the literature. Hyer (1982) first determined the solution for a rectangular cross-ply laminate. A cross-ply laminate is fabricated by stacking uniaxial fiber reinforced composite layers in orthogonal directions in the upper and lower halves of the plate. Because of the substantial anisotropy in the thermal expansion of the laminae, thermal expansion induced deformation is initially saddle-shaped, and exhibits a bifurcation into a cylindrical form. Notably the cylindrical secondary solution here is the same general shape as in the isotropic case. Masters and Salamon (1993) modified the Hyer result by introducing additional degrees of freedom into the assumed deformation form, resulting in an improved prediction of the bifurcation point without significantly increasing the complexity of the calculation. Freund (2000) extended these results to the problem of a thin film on a circular plate.

Recently, thermally induced plate warping was again observed experimentally and compared with the known solutions (Parthasarathy, Keller, et al , 2004). In this case, square plates of ceramic-fiber woven cloth embedded in a ceramic matrix were fabricated. The cloth contained equal number of fibers in each direction and the composites were fabricated with a '0/90' layup. Fibers with different thermal expansion and elastic response were used in the upper and lower half of the plate. On cooling from processing temperatures the plates warped to a cylindrical shape for 'large' plates (Figure 2) and a spherical shape for 'smaller' samples. Note in this case the elastic response is square-symmetric (within each layer the elastic moduli are equal in each direction parallel to the plate edges). It is not, however, isotropic as the modulus in the 45 degree orientations is lower than in the 0/90 directions. The reduction in shear modulus in this example is small so that isotropy was assumed in comparing the experiment with analytic results. The thermal straining is symmetric and uniform in each layer and the spherical small strain result that was observed is in fact what is predicted analytically.

Interestingly, however, while the observed cylindrical large-strain mode appears to be in agreement with the analyses, the cylindrical bifurcation mode differs subtly from the predictions. Note in Figure 2b that, while the plate curvature is cylindrical, the cylinder axis is aligned with a plate diagonal rather than a plate edge. This deformation mode clearly exists in this case because, owing to the square symmetry of the plate, the plate diagonals also represent symmetry planes for the deformation.

The present analysis is a modification of the Masters and Salamon analysis procedure that reveals the 'new' bifurcation mode and shows clearly why this is observed only for an orthotropic plate. The paper is organized as follows: first we review in some detail the existing models, then we present the new analytic solution. Because the analytic results only predict the *existence* of multiple equilibrium

solutions, in the following section the stability of the various solution is examined numerically. Next a finite element simulation is presented for comparison and verification, and finally the extension of the analytic method to high order polynomial forms is investigated.

Parallel mode bifurcation

The bifurcation analysis proceeds by development of approximate displacement functions, calculation of the associated elastic strain energy and application of the minimum potential energy theorem to determine if one or more equilibrium solutions exists. Note that the results are approximate and limited to the function space of the assumed displacement functions. In order to obtain closed form results the simplest possible displacement functions are desired, and so it is helpful to know *a priori* the form of the displacement and construct displacement functions that capture the expected result. However the present analysis is an example where an unexpected bifurcation mode is missed as a result of the selection of approximating functions

Both Hyer and Masters and Salamon analyze the plate problem by assuming an out-of-plane displacement $w^p(x,y)$ of the form,

$$w^p(x,y) = \frac{1}{2h}\left(ax^2 + by^2\right) \tag{1}$$

where h is the plate thickness, x and y are the in-plane coordinates in an axis system centered at the plate centroid and aligned with the plate edges (or with the principal axes of the material orthotropy when considering circular plates). The dimensionless constants a and b are to be determined. By construction, a/h and b/h are the principal curvatures at the center of the plate. Clearly, this form admits the spherical mode with, $a = b$ the saddle mode with $a = -b$, and cylindrical modes when one of a or b is zero. As noted, the "cylindrical" mode is actually more closely approximated as an ellipse with $a \neq b$, and one of the principle curvatures tending to zero for large strain. It is apparent that the diagonally-oriented-cylinder mode was not anticipated and hence is precluded from these solutions.

Using symmetry arguments, Masters and Salamon propose general in-plane displacements of the form,

$$\begin{aligned} u^p(x,y) &= d_1^p x + d_2^p x^3 + d_3^p xy^2 \\ v^p(x,y) &= d_4^p y + d_5^p y^3 + d_6^p yx^2 \end{aligned} \tag{2}$$

where u^p and v^p are the x- and y-displacements of the plate mid-plane, and the d_i^p represent six additional constants to be determined. Note that a and b have been eliminated from the in-plane displacement form used by Masters and Salamon without loss of generality.

The strains throughout the plate are then calculated using Kirchoff plate theory (Vinson and Chou, 1975),

$$\varepsilon_x = \frac{\partial u}{\partial x} + \frac{1}{2}\left(\frac{\partial w}{\partial x}\right)^2 - z\frac{\partial^2 w}{\partial x^2}$$
$$\varepsilon_y = \frac{\partial v}{\partial y} + \frac{1}{2}\left(\frac{\partial w}{\partial y}\right)^2 - z\frac{\partial^2 w}{\partial y^2} \qquad (3)$$
$$\gamma_{xy} = \frac{\partial u}{\partial y} + \frac{\partial v}{\partial x} + \frac{\partial w}{\partial x}\frac{\partial w}{\partial y} - 2z\frac{\partial^2 w}{\partial x \partial y}$$

where z is the thickness coordinate. Hyer's calculation is a special case where $\gamma_{xy} = 0$ is prescribed on the mid-plane $(z = 0)$ by setting $d_3^p = d_6^p = -ab/4h^2$. Note however that this (ad hoc) constraint equation ultimately results in only a minimal algebraic simplification when compared to the full (i.e. Masters and Salamon's "case 3") solution. Indeed closed form solutions may be obtained with even more degrees of freedom introduced in the in-plane displacements, as will be discussed in a later section.

The material constitutive response is written in 'reduced' composite laminate notation (Vinson and Chou, 1975),

$$\begin{bmatrix} \sigma_x \\ \sigma_y \\ \sigma_{xy} \end{bmatrix} = \begin{bmatrix} Q_{11} & Q_{12} & 0 \\ Q_{12} & Q_{22} & 0 \\ 0 & 0 & Q_{66} \end{bmatrix} \begin{bmatrix} \varepsilon_x - \varepsilon_x^t \\ \varepsilon_y - \varepsilon_y^t \\ \gamma_{xy} \end{bmatrix} \qquad (4)$$

where the material constants Q_{ij} and the thermal strains $\varepsilon_x^t, \varepsilon_y^t$,are variable through the thickness but constant over the plate area. The strain energy is then,

$$\Psi = \int_{-h/2}^{h/2} \int_A \frac{1}{2} Q_{11}\left(\varepsilon_x - \varepsilon_x^t\right)^2 + \frac{1}{2} Q_{22}\left(\varepsilon_y - \varepsilon_y^t\right)^2 + \frac{1}{2} Q_{12}\left(\varepsilon_x - \varepsilon_x^t\right)\left(\varepsilon_y - \varepsilon_y^t\right) + 2Q_{66}\gamma_{xy}^2 \, dA dz \qquad (5)$$

where the inner integral is taken over the plate area A. Because the Q_{ij} are functions of z only this can be integrated explicitly, in terms of the plate stiffness matrices (**A**,**B**,**D**) which are given in the appendix. The theory of minimum potential energy requires that, for an equilibrium solution, $\delta\Psi = 0$ (Sokolnikoff, 1956), hence,

$$\frac{\partial \Psi}{\partial a} = \frac{\partial \Psi}{\partial b} = 0 \qquad (6a)$$

$$\frac{\partial \Psi}{\partial d_i^p} = 0 \qquad i = 1,6 \qquad (6b)$$

Expression (6b) is a system of six equations which are linear in the six d_i^p, and quadratic in a and b, hence the d_i^p may be directly expressed in terms of a and b. Upon substitution, eq (6a) is then a pair of nonlinear expressions in a and b only,

$$a = -\frac{G_1 b + hG_2}{G_3 (b/h)^2 + G_4} \quad b = -\frac{H_1 a + hH_2}{H_3 (a/h)^2 + H_4} \tag{7}$$

where G_i, H_i are the algebraic functions of the material properties and plate dimensions given in Masters and Salamon (1993). The system has either one or three real solutions corresponding to the primary and secondary deformation modes.

At this point we will specialize to the case of square symmetry. That is, the material constants are all symmetric with respect to a 1-2 transformation ($Q_{11} = Q_{22}$, etc), the thermal strain is symmetric, $\varepsilon_y^t = \varepsilon_x^t \equiv \varepsilon^t$ and the *geometry* is square-symmetric. Note that the plate need not be a square, i.e. a circular plate also has the required symmetry. The material response may be non-isotropic with $Q_{66} \neq (Q_{11} - Q_{12})/2$. For this symmetry, Masters and Salamon's "isotropic simplification" may be utilized directly, noting that they only require the 1-2 symmetry. That is, their result is more general then they asserted. For this case, $G_i = H_i$ for all *i* in (7). The expressions thus may be combined to form a fifth order polynomial in *a,*

$$\left(H_2^\varepsilon + \left(H_1^* + H_4^*\right)a + L^{*4} H_3^* a^3\right)\left(H_4^*\left(H_4^* - H_1^*\right)/\left(H_3^* L^{*4}\right) + H_2^\varepsilon a + H_4^* a^2\right) = 0 \tag{8}$$

and an identical polynomial in *b*. This is the result obtained by Masters and Salamon, however for convenience we have defined H_i^* and H_2^ε so that all of the "*H*" constants have equal dimension and depend only on the section properties and the shape (not size) of the plate. L^* is the dimensionless size of the plate; $L^* = L/h$ for a square with edge length *L* and is likewise L^* is the normalized diameter for a circular plate. The superscript, ε, has been introduced to indicate that *only* H_2^ε depends on the thermal strain. Expressions for the square-symmetry H_i^*, for square and circular plates, are given in the appendix.

The cubic factor in Eq. (8) always has one real root corresponding to the $a = b$ primary solution, noting that the same cubic is obtained by setting $a = b$ in Eq. (7). For typical stable materials and grading, $H_3^* > 0$ and $H_4^* > H_1^* > 0$ and it is readily shown that there is exactly one root.

The quadratic factor has two real roots only if

$$\left(L^{*2} H_2^\varepsilon\right)^2 \geq 4\left(H_4^*\right)^2\left(H_4^* - H_1^*\right)/H_3^* \tag{9}$$

Where the equality is satisfied, Eq (8) has a triple root at $a = -H_2^\varepsilon / 2H_4^*$. This is the loss of uniqueness, or bifurcation point. The right side of (9) is notably dependant only on the shape of the plate and the section properties. The thermal strain only appears in H_2^ε, hence the critical thermal strain required for the loss of uniqueness is given in closed form. For larger $L^{*2} H_2^\varepsilon$ the quadratic formula yields two real solutions which are the major and minor axis of the elliptical deflection. In the large strain limit the

curvatures asymptote to 0 and $a = -H_2^{\varepsilon} / H_4^*$. The elastic stability of the solutions is discussed in a subsequent section.

Diagonal mode bifurcation

As noted, the assumed deformation form, Eqn's (1) and (2), permits only the primary and edge-parallel cylinder modes. In order to examine the diagonal mode we assume displacement forms that admit the observed shape. Equation (1) is replaced with,

$$w^d(x,y) = \frac{1}{4h}\left(a(x+y)^2 + b(x-y)^2\right) \tag{10}$$

where the constants, *a* and *b*, to be determined, again are the dimensionless principal curvatures of the deformed shape. In this case, of course, the principal curvature axes are aligned with the plate diagonals. Note that here we have obviously precluded the edge-parallel bifurcation modes, however, as with the parallel mode form, $a = b$ corresponds to the primary 'bowl' shape. This approach is followed because solving the diagonal mode problem separately leads to closed form results, while solving the minimization problem for a more general displacement form, with an additional constant that would permit both modes, does not.

It may be noticed that the 'diagonal' bifurcation solution could equivalently be obtained as a 'parallel' bifurcation of a diagonally-oriented plate, by transforming the Q matrix as well as the area of integration in Eq (5). The approach adopted here is no more cumbersome and will facilitate investigation of the stability of the combined-mode problem.

Noting that we are here considering only the square symmetry case, for diagonal displacement symmetry, the in-plane displacements must satisfy, $u(x,y) = -u(-x,-y)$ and $v(x,y) = u(y,x)$ hence the trial displacement form used is,

$$\begin{aligned} u^d(x,y) &= d_1^d x + d_2^d x^3 + d_3^d xy^2 + d_4^d y + d_5^d y^3 + d_6^d yx^2 \\ v^d(x,y) &= d_1^d y + d_2^d y^3 + d_3^d yx^2 + d_4^d x + d_5^d x^3 + d_6^d xy^2 \end{aligned} \tag{11}$$

Note that we have the same number of unknowns as in the parallel-mode analysis. Following the identical procedure we arrive at essentially the same form as Eqn's (7) and (8)

$$a = -\frac{\left(H_1^* - \lambda\right)b + H_2^{\varepsilon}}{L^{*4} H_3^* b^2 + \left(H_4^* + \lambda\right)} \qquad b = -\frac{\left(H_1^* - \lambda\right)a + H_2^{\varepsilon}}{L^{*4} H_3^* a^2 + \left(H_4^* + \lambda\right)} \tag{12a}$$

$$\left(H_2^{\varepsilon} + \left(H_1^* + H_4^*\right)a + L^{*4} H_3^* a^3\right)\left(\left(H_4^* + \lambda\right)\left(H_4^* - H_1^* + 2\lambda\right)/\left(H_3^* L^{*4}\right) + H_2^{\varepsilon} a + \left(H_4^* + \lambda\right)a^2\right) = 0 \tag{12b}$$

Where the H_i^* are the same as in Eq (8), and

$$\lambda = \frac{(A_{11}+A_{12})}{h^5}\left(2B_{66}^2\left(\left(\frac{B_{11}-B_{12}}{2B_{66}}\right)^2 - \frac{A_{11}-A_{12}}{2A_{66}}\right) + (A_{11}-A_{12})D_{66}\left(1-\frac{D_{11}-D_{12}}{2D_{66}}\right)\right) \tag{13}$$

recalling that **A**,**B**,**D** are the plate stiffness matrices as-defined in the appendix. Clearly then, comparing (8) and (12b), the cubic factor is the same and is likewise obtained by setting a=b in (12a) so that the primary solution displacement field is identical to that of the parallel mode analysis. Multiple solutions exist when the quadratic part of 12b has real roots hence,

$$\left(L^{*2}H_2^{\varepsilon}\right)^2 \geq 4\left(H_4^* + \lambda\right)^2\left(H_4^* - H_1^* + 2\lambda\right)/H_3^* \tag{14}$$

In order to illustrate the physical significance of λ, assume that throughout the plate the in-plane shear stiffness is given by,

$$Q_{66} = \frac{\phi}{2}(Q_{11} - Q_{12}) \tag{15}$$

where ϕ is an arbitrary constant, with $\phi = 1$ resulting in isotropy, then we will have, from Eq. (A1) $A_{66} = \phi(A_{11}-A_{12})/2$, $B_{66} = \phi(B_{11}-B_{12})/2$, and $D_{66} = \phi(D_{11}-D_{12})/2$ so that,

$$\lambda = \frac{(\phi-1)}{2}\frac{A_{11}+A_{12}}{h^5}\left[(A_{11}-A_{12})(D_{11}-D_{12}) - (B_{11}-B_{12})^2\right] \tag{16}$$

Thus λ can be seen as an indicator of isotropy; negative where the plate shear modulus is lower than the equivalent isotropic value and positive if the plate has high in-plane-shear stiffness. (The quantity in [ ] is strictly positive for stable materials).When the elastic response is isotropic, $\lambda = 0$ so that Eq (8) and Eq(12b) are identical and predicted bifurcation points are the same for both modes. As will be discussed in the simulation section, however, this exact coincidence of the two solutions is an artifact of the approximating functions selected.

For nonzero λ *both* parallel and diagonal modes must be considered. A loss of uniqueness occurs when either of the conditions (9) or (14) is satisfied. When both inequalities are satisfied there are five equilibrium solutions. Comparing Eq. (9) and Eq. (14) it can easily be shown that so long as $H_3^* > 0$ and $H_4^* > H_1^* > 0$ then a negative λ (i.e. low in-plane shear stiffness) results in the diagonal mode occurring at a lower thermal strain and a positive λ results in the parallel mode occurring first.

Example and comparison with experiment

Oxide fibers offer a convenient approach to validate the model developed in this work. In particular, oxide fibers from 3M, Inc., range in modulus from about 150 GPa to 380 GPa and thermal expansion coefficient from 4 to 8.3 ppm/C. Among these fibers, Nextel610 and Nextel720 fibers are most resistant to high temperature treatments. Nextel610 has a modulus of 380 GPa and CTe of

8.3ppm/C, while Nextel720 has a modulus of 262 GPa and a CTE of 6.5 ppm/C. To validate the model predictions, composites that contained Nextel610 fibers on one half of its thickness, and nextel720 fibers on the other half were considered. Porous alumina matrix composites were prepared using 2D woven cloths of Nextel610 and Nextel720 fibers. They were processed at high temperature (~1200C) to densify the matrix. At the end of sintering at this temperature the entire composite is in the iso-strain condition. Upon cooling to room temperature the difference in modulus and CTE results in a gradient of CTE-mismatch induced strain. This strain results in a bending of the composite laminate.

Two size of composites were fabricated. One of them was a circular plate that was 0.12 m (4,75") in diameter. This was fabricated using a layup of woven (8HS) cloths of the two fibers, Nextel610 and Nextel720 (3M corp.). The cloths were cut into 127mm (5") diameter and stacked. 3 plies of Nextel610 fiber cloth was stacked on top of 3 plies of Nextel 720 fiber cloth. The cloths were desized at 600C, 1h in air, before infiltrating with a slurry of alumina powder (AKP-53, Sumitomo, Inc.). Final sintering was done at 1200C, 5hrs in air. The composite was slow cooled with the furnace..

The second set of composites were made to prescribed composition of fibers by COI, Inc. (now ATK-COI). The composition was the same as the smaller sample, but the size was larger and the shape was square. Plates of dimensions 152mm x 152 mm (~6"x6") were fabricated and sintered at an undisclosed temperature, but close to 1200C.

The as-fabricated samples showed distortion resulting from CTE mismatch upon cooling from processing temperature. The circular disc that was 120 mm in diameter exhibited a symmetric spherical distortion, while the 152 mm square disc exhibited an asymmetrical distortion, with the undistorted line following the diagonal of the square.

Consider a square plate of thickness $h = 1.25mm$ and variable edge length L. Assume two equal-thickness layers, with elastic constants given by,

$$Q_{11} = Q_{22} = \begin{cases} 3/4\Sigma & 0 < z < h/2 \\ \Sigma & -h/2 < z < 0 \end{cases}$$

$$\begin{aligned} Q_{12} &= \nu\ Q_{11} \\ Q_{66} &= \frac{\phi(1-\nu)Q_{11}}{2} \end{aligned} \qquad (17)$$

where ν is Poisson's ratio, Σ is the uniaxial stiffness of the lower lamina. For simplicity of example we take $\nu = 0.1$ thought the thickness and note that Σ need not be specified as it factors out of the analysis. The CMC experiment shown in Figure 2 is approximated by setting $\phi = 0.4$, while $\phi = 1$ indicates isotropy.

Further, assume the thermal strains are similarly graded as

$$\varepsilon_x^t = \varepsilon_y^t = \begin{cases} 3/4\,\alpha\,\Delta T & 0 < z < h/2 \\ \alpha\,\Delta T & -h/2 < z < 0 \end{cases} \tag{17a}$$

where α is thermal expansion coefficient of the lower plate half, taken to be $\alpha = 8 \cdot 10^{-6} / {}^{\circ}C$ for this example and ΔT is a prescribed temperature change.

Figure 3 shows the isotropic $(\phi = 1)$ solution, for $L = 150mm$ which is, since $\lambda = 0$, the same for either mode. The asymmetric expansion plate, when heated or cooled through a uniform temperature change of $486\ {}^{\circ}C$ or greater is predicted to deform to a cylindrical shape. The stability of the solutions, indicated by the line types on the figure will be discussed in a subsequent section.

Figure 4 shows the effect of reducing the shear modulus of the plate by setting $\phi = 0.4$, approximating the CMC experiment. The location of the equivalent isotropic bifurcation point is shown for reference. Reducing the shear modulus increases the primary mode deflection slightly, as A_{66} appears in the constant H_3^*, however the affect on the bifurcation solutions is far more significant. The edge-parallel mode shifts upward by $\sim 100\ {}^{\circ}C$ and the diagonal mode shifts downward nearly $\sim 300\ {}^{\circ}C$, so that the diagonal mode is the one that will appear first.

Figure 5 shows the sensitivity of the critical point to the plate orthotropy. For a plate where the in-plane shear is equal-to or greater-than the corresponding isotropic shear stiffness the lower (i.e. design limiting) bifurcation is always the parallel one and further there is very little sensitivity to increasing stiffness. Hence the isotropic assumption is a good approximation. On the other hand, for reduced shear, as is common with "0/90" composites, the critical thermal strain resulting from the diagonal mode drops off sharply, hence the isotropic assumption may seriously overestimate the critical condition.

Figure 6 shows the trend in the solutions with the size of the plate. The plate size appears only in the left term of Eq. (9) and Eq. (14) and, in this example, H_2^{ε} is linear in the thermal strain, hence the critical strain varies simply as $(h/L)^2$. From this figure we can identify the critical plate size where instability occurs. Figure 6 also shows the critical temperature variation with diameter for circular plates. For the same dimension, diameter or edge length, circular plates are somewhat more stable.

If we consider now the motivating experimental results we can show only an approximate correlation. The model correctly predicts a diagonal deformation of the square plate, however the critical size for a circular plate is predicted to be only 80mm diameter. There are several reasons for this. Principally as will be discussed in the simulation section, the bifurcation analysis tends to be conservative. The true critical size for a specified thermal strain will be somewhat larger than predicted. Additionally, the material properties are idealized approximations. In particular, the actual difference in thermal expansion between the plys in the composite is likely somewhat smaller than assumed in the simulation,

making the prediction even more conservative. None the less the critical size is the correct order of magnitude, and more importantly the diagonal form is correctly predicted for the square plate.

Stability

The results obtained thus far show only the existence of multiple solutions. In order to evaluate the stability of the solutions we must construct the Hessian matrix,

$$\left[\frac{\partial^2 \Psi}{\partial p_i p_j}\right] \qquad i,j = 1,N \tag{18}$$

where the p_i represent all of the N unknowns for the respective solution (i.e. $p_1 = a, p_2 = b, p_3 = d_1 \ldots$) When the Hessian matrix is positive definite the solution is a local minima of the energy function, hence a stable solution. Unfortunately, algebraically evaluating the positive definiteness of the matrix is not tractable, so we proceed by populating the matrix using the analytic solutions and then numerically evaluating determinants of all of its principal minors. Using this procedure both the parallel and diagonal solutions, considered separately, exhibit the expected 'exchange of stability' behavior typical of such elastic bifurcations (Thompson and Hunt, 1973). That is, the primary mode is stable up to the bifurcation point, beyond which the primary mode looses stability and each of the complementary asymmetric solutions is stable. Its important to note however that this stability determination is valid only for deformation restricted to the assumed function space. In other words, it is possible that an unstable configuration is erroneously predicted to be stable because we not have not used sufficiently general trial functions.

In order to address the combined stability consider a displacement form which is sufficiently general to include either parallel or diagonal bifurcation modes,

$$w^*(x,y) = \frac{1}{2h}\left(a^* x^2 + b^* y^2 + c^* xy\right) \tag{19}$$

$$\begin{aligned} u^*(x,y) &= d_1^* x + d_2^* x^3 + d_3^* xy^2 + d_7^* y + d_8^* y^3 + d_9^* yx^2 \\ v^*(x,y) &= d_4^* y + d_5^* y^3 + d_6^* yx^2 + d_7^* x + d_8^* x^3 + d_9^* xy^2 \end{aligned} \tag{20}$$

and let $\Psi^* = \Psi\left(w^*, u^*, v^*\right)$ be the associated potential energy functional. Stationary solutions for Ψ^* are found by solving $\partial\Psi^*/\partial a^* = \partial\Psi^*/\partial b^* = \partial\Psi^*/\partial c^* = \partial\Psi^*/\partial d_i^* = 0$ to eliminate the d_i^* as before. The resulting three nonlinear equations in a^*, b^*, c^* are not readily solvable, however it can be shown that each of the solutions to the separate-mode problems also satisfies the stationary condition for the *combined mode* problem, i.e. with $a^* = a, b^* = b$ while $c^* = 0$ for parallel solution and $c^* = a - b$ for diagonal. The algebra required to show this is lengthy but straightforward. Of course it is plausible that

even more solutions exist for the formulation with three degrees of freedom in the out of plane deformation, however numerical investigation did not reveal any new modes.

For each of the known solution, the Hessian matrix of the Ψ^* function must be checked for positive definiteness. For the isotropic case the result is always the same as was found for the separate modes, that is each of the asymmetric modes is stable for any thermal strain beyond the shared bifurcation point. Indeed both modes show the same strain energy at any point along the curve, and so there is nothing to indicate that one solution should be favored. However as will be discussed in the next section, the fact that the two modes show precisely the same bifurcation point is an artifact of the chosen displacement forms.

In the anisotropic case, there are two different bifurcation points. As may be expected the solution that exhibits the lower bifurcation (i.e. diagonal in the $\lambda<0$ example) exhibits the usual exchange of stability and the bifurcation solution remains stable for large thermal strains. However, the mode that occurs later (parallel) *also* looses stability at the *lower* bifurcation point when the combined displacement function is considered. That is, between the two bifurcation points the solution appears to be stable if the existence of the first mode is ignored but is actually unstable. This condition is denoted quasi-stable on Figure 4. Interestingly, somewhat beyond its bifurcation point, the parallel curvature solution regains stability, that is, it is a local minima of the combined problem. The potential Ψ^* is however always lower for the diagonal mode, making it the global minimum.

Simulation

In order to confirm the results, the analysis was duplicated using an ABAQUS finite element model (ABAQUS, 2004). Figure 7a shows the primary deformation mode for the plate, using a mesh of 1000 shear-deformable-shell-elements (type S4). As is typical, the FEM solution does not reveal the instability of the primary solution and so only this mode is obtained from a simple direct analysis.

A common procedure to investigate bifurcation behavior is to impose some defect into the plate at zero temperature to force the solution to the asymmetric modes (see e.g. 1994 Masters and Salamon, 1994). However, in this case, because there are two sets of solutions it would not be possible to study that quasi-stable secondary bifurcation behavior, thus an alternate approach is suggested.

The secondary solutions are obtained by first applying displacement boundary conditions to 'bend' the plate into the expected shape, i.e. to simulate the parallel mode a line of nodes along y=0 is fixed and the edge nodes along y=+/-L/2 are displaced uniformly by the amount given by Eq (1) along with the predicted principal curvature at some temperature, Tmax , well above the expected bifurcation point. Tmax is then applied uniformly to the plate. As a third step the 'seed' displacement conditions are removed (except as needed to eliminate rigid body displacement). The validity of the analytic results are

supported by the fact that the plate remains in the imposed cylindrical shape when the forcing displacement conditions are removed. For Tmax sufficiently large that *both* (9) and (14) are satisfied, *either* mode is shown as a valid equilibrium solution in this manner. It is notable that the seed displacement conditions need not be exact. Indeed by applying approximate displacements and observing that the numerical solution takes on the predicted form we have an indication (though not proof) of the stability of the configuration. As predicted analytically, both shapes are sufficiently stable for sufficiently high temperatures that any reasonable approximation will drive the numerical solution into those forms. Figures 7b and 7c show the simulated parallel and diagonal cylinder configurations.

From the initial high temperature, the temperature is ramped *down* in small increments to zero. For each increment, the principle curvatures are determined by least squares fits of the appropriate form, Eq. (1) or Eq (10), to the nodal displacements derived from the finite element analysis.

Figure 8 shows the simulated results using the same material parameters as in the previous isotropic example, hence may be compared directly with Figure 3. The parallel mode shows reasonable agreement for the isotropic case, with the difference between analytic and numerical results comparable to that found by Masters and Salamon (1993).

The numerically-derived diagonal-mode bifurcation point is, however, higher than the parallel, thus contradicting the analytic prediction that the two cases should be identical. Qualitative insight into this issue is gleaned by

Note that the finite element results are, of course, also approximations. However, the significant difference in the methods lies in the fact that the analytic results are restricted to quadratic out-of-plane approximate displacement while the finite element method can approximate an arbitrary form using a much greater number of degrees of freedom. By comparing the numerical solutions with the least-squares quadratic form fits that were used to determine their curvatures, we find that in for both modes the fits are qualitatively quite good -- that is the two modes are indeed well approximated by the forms (1) and (10). However the FEM solution reveals deviation from the simple polynomial displacement form, especially near the edges and corners of the square plate. Further, the deviation from the quadratic from is more significant for the diagonal mode than for the parallel mode. On this bases we will conclude that the FEM predictions are the most accurate, and that between the two analytic solutions we expect that the parallel mode solution is somewhat more accurate.

We can conclude then, as noted previously, that the 'exact' coincidence of the analytic predictions for an isotropic plate is an artificial result of one solution using a marginally more accurate trial function than

the other. This conclusion is further supported by the fact that no evidence has been found in the literature of an observation of a diagonal bifurcation in an isotropic plate.

The 'new' solution is, nonetheless, quite valuable when any anisotropy is taken into account. Figure 9 shows the finite element simulation for a low in-plane shear stiffness plate (ϕ=0.4). The numerical simulation shows the same shifting of the two solutions' bifurcation points in opposite directions as was predicted by the analysis.

Higher order improved accuracy solutions.

In an effort to close the difference between the finite element and analytic results, improved accuracy solutions are obtained by using higher order polynomials in the trial functions. Such higher order solutions were obtained for the parallel mode bifurcation by Salamon and Masters (1994) using 6th order polynomials in the strain, or equivalently 7th order displacement functions. Unfortunately, as was noted in the stability analysis section, introducing more than two degrees of freedom in the out of plane displacement function results in an unwieldy system or nonlinear equations. The in-plane displacements *u(x,y)* and *v(x,y)* may in, however be expanded in arbitrary polynomials in *x* and *y*. For any polynomial form, all of the unknown coefficients ultimately appear linearly in the variational statement, hence they may always be (in principle) algebraically eliminated to produce a pair of nonlinear equations in the principal curvatures (*a* and *b*). Here we examine the convergence of the solutions for increasing order of in-plane displacement functions.

For the parallel mode deformation, using symmetry arguments, we require only odd powers of *x* and even powers of *y* in the *x*- displacement and likewise odd powers of *y* and even powers of *x* in the *y*-displacement. The following construction results in polynomial expressions containing all such terms up to a power of $2N+1$.

$$\begin{aligned} u^p(x,y) &= \sum_{j=0,N}\sum_{i=0,N-j} f_{I^p(i,j)} x^{2i+1} y^{2j} \\ v^p(x,y) &= \sum_{j=0,N}\sum_{i=0,N-j} f_{I^p(i,j)+1} y^{2i+1} x^{2j} \end{aligned} \tag{20a}$$

where I^p is an index function constructed to assign unique indices to each of the coefficients, f,

$$I^p(i,j) = j(2N+3-j)+2i+1 \tag{20b}$$

Expansion of Eq. (20a) results in *(N+1)(N+2)* unknowns. Note that *N=1* produces trial displacement forms equivalent to Eq(2) and *N=3* results in Masters and Salamon's "expanded" order formulation.

For the diagonal mode, again using symmetry arguments, we obtain the expressions,

$$u^d(x,y) = \sum_{j=1,N+1} \sum_{i=1,2j} g_{I^d(i,j)} x^{i-1} y^{2j-i}$$
$$v^d(x,y) = \sum_{j=1,N+1} \sum_{i=1,2j} g_{I^d(i,j)} y^{i-1} x^{2j-i} \qquad (20c)$$
$$I^d(i,j) = j(j-1)+i$$

In this case, each displacement function has *(N+1)(N+2)* terms, however the coefficients, *g,* are shared so that the same number of undetermined coefficients results. Likewise *N=1* results in the cubic form (11).

For both parallel and diagonal modes, combining these high order expansions with the appropriate out-of-plane expression, (1) or (10), results in a system of nonlinear equations that may be (in principle) algebraically reduced to the form (8). Improved accuracy solutions are thus obtained. The resulting expressions for the "*H*" constants become increasingly unwieldy with large *N*, however. In fact for *N>3* it becomes impractical to solve the linear system equivalent to Eq (6b) even with a computer symbolic algebra package. Hence for large *N* we have used numerical methods to generate results for a specific example.

It should be mentioned that imposing symmetry on the displacement approximation serves only to simplify the algebra and eliminate rigid body displacement. As there are no displacement boundary conditions, the minimum energy principle requires only continuous, differentiable displacement approximating functions. Any asymmetric terms, if included, will naturally cancel from the analysis. Further, there is no reason, other than algebra reduction, to impose edge conditions on the displacement. For example imposing zero shear *strain* on a *stress free* edge is not necessary, although such approximations may lead to algebraic formulations that can reasonably be solved by hand (Hyer,1982). In the present analysis no such extra approximations are made, however our approach is essentially dependant on the use of computational symbolic algebra routines, and even, as noted, numeric methods for large *N*.

Figure 10 shows that for increasing polynomial order the bifurcation predictions converge to fixed values. It is readily apparent that the seventh order result is sufficient and that negligible gains are made with larger *N*. It is also apparent that the analysis results *do not* converge exactly to the finite element derived results. This is readily seen as a result of the fact that we are not adding additional degrees of freedom to the out-of-plane trial functions. From this we can conclude that it is not worthwhile to expand the in-plane trial functions to much higher order than the out-of-plane trial functions.

Closure

It has been shown, for the special case of thin plates with square-symmetry, an additional bifurcation mode becomes available. Most significantly, for the case of '0/90' composites, where the in-plane shear

modulus is typically relatively low, the new mode occurs at much lower mismatch strain than predicted by prior analysis. The analytic method presented here provides a conservative estimate of the critical condition as well as a procedure for demonstrating the stability of the various solutions.

Acknowledgment

This work was performed while one author (G.J.) held a National Research Council Research Associateship Award at the Air Force Research Laboratory Materials and Manufacturing Directorate.

References

ABAQUS Analysis Users Manual, Version 6.4, 2003, ABAQUS, Inc, Pawtucket, RI.

Freund, L.B. Substrate curvature due to thin film mismatch strain in the nonlinear deformation range. Journal of the Mechanics and Physics of Solids. 48 1159-1174 (2000)

Hyer, M.W. The Room -Temperature shapes of four-layer unsymmetric cross-ply laminates. Journal of Composite Materials, 16 318-340 (1982)

Masters, C.B., and Salamon, N.J., Geometrically nonlinear stress-deflection relations for thin film/substrate systems, International Journal of Engineering Science, 31 [6] 915-925 (1993).

Parthasarathy, T.A., Keller, K.A., Mah, T-I, Kerans, R.J., and Butner, S. Reduction of Thermal-Gradient-Induced Stresses in Composites Using Mixed Fibers, *J. Am. Ceram. Soc.,* 87 [4] 617–25 (2004)

Salamon, N.J., and Masters C.B., Geometrically Nonlinear Stress-Deflection Relations for Thin Film/Substrate Systems With a Finite Element Comparison, Journal of Applied Mechanics **61** 872-878 (1994)

Salamon, N.J., and Masters C.B., Bifurcation in Isotropic Thin Film/Substrate Plates, International Journal of Solids and Structures **32** [3-4] 473-481 (1995)

Sokolnikoff, I.S., Mathematical Theory of Elasticity, McGraw Hill, New York (1956)

Thompson J.M.T and Hunt, G.W A General Theory of Elastic Stability. John Wiley, New York (1973)

Vinson, J.R. and Chou, T-W. Composite Materials and their use in Structures. John Wiley, New York. (1975)

Appendix 1

The components of the laminate stiffness matrix are defined as (Vinson, 1986),

$$A_{ij} = \int_{-h/2}^{h/2} Q_{ij}\,dz \quad B_{ij} = \int_{-h/2}^{h/2} Q_{ij} z\,dz \quad D_{ij} = \int_{-h/2}^{h/2} Q_{ij} z^2\,dz \tag{A1}$$

The forces and moments (per unit width) in the plate associated with the thermal strain for the special case of square symmetry are,

$$N^t = \int_{-h/2}^{h/2} (Q_{11} + Q_{12})\varepsilon^t dz \quad M^t = \int_{-h/2}^{h/2} (Q_{11} + Q_{12})\varepsilon^t z\,dz \tag{A1a}$$

Square symmetry *H* constants. Non-superscripted quantities are Masters and Salamon's "isotropic case 3" constants. The corresponding superscripted quantities are normalized to have equal dimension (stress cubed). Three of the constants are dependant only on the section properties.

$$\begin{aligned} H_1^* &= H_1/h^5 = (1/h^5)\left(D_{12}\left(A_{11}^2 - A_{12}^2\right) - 2A_{11}B_{11}B_{12} + A_{12}\left(B_{11}^2 + B_{12}^2\right)\right) \\ H_2^{\varepsilon} &= H_2/h^4 = (1/h)^4 (A_{11} - A_{12})\left[(A_{11} + A_{12})M^t - (B_{11} + B_{12})N^t\right] \\ H_4^* &= H_4/h^5 = H_1^* + (1/h^5)(A_{11} + A_{12})\left[(D_{11} - D_{12})(A_{11} - A_{12}) - (B_{11} - B_{12})^2\right] \end{aligned} \tag{A2}$$

The fourth constant depends on the shape of the plate.

For a square plate, edge length *L*,

$$H_3^* = H_3/\left(h^7 L^{*4}\right) = \frac{\left(A_{11}^2 - A_{12}^2\right)^2}{144h^3}\left(\frac{A_{11}^2 - A_{12}^2}{A_{66}} + 10A_{11}\right)^{-1} \tag{A2a}$$
$$L^* \equiv L/h$$

For a circular plate of radius R

$$H_3^* = \frac{\left(A_{11}^2 - A_{12}^2\right)^2}{h^3 384}\left(\frac{A_{11}^2 - A_{12}^2}{A_{66}} + 6A_{11} - 2A_{12}\right)^{-1} \tag{A3}$$
$$L^* = 2R/h$$

For a circular ring of outer radius *R* and inner radius $R_0 = \xi R$

$$H_3^* = \frac{\left(A_{11}^2 - A_{12}^2\right)^2\left(1 + \xi^2 + \xi^4\right)}{384h^3}\left(\frac{A_{11}^2 - A_{12}^2}{A_{66}} + 6A_{11} - 2A_{12} + 12(A_{11} - A_{12})\left(\frac{\xi}{1 - \xi^2}\right)^2\right)^{-1} \tag{A4}$$

$$L^* = 2R/h$$

Appendix 2 Uniform elasticity case.

For completeness, and to illustrate the calculation, consider the problem posed by Freund (2000) of a two-layer circular plate with uniform elastic response throughout. That is for all z,

$$Q_{12} = \nu\ Q_{11}$$
$$Q_{66} = \frac{\phi(1-\nu)}{2} Q_{11} \tag{A5}$$

where ν is Poisson's ratio. The constant Q_{11} may be written in terms of Poisson's ratio and Young's modulus, *E*, however it factors out of all of the relevant expressions. A constant mismatch strain is specified in one layer relative to the other

$$\varepsilon_x^t = \varepsilon_y^t = \begin{cases} \varepsilon_s + \varepsilon_m & -h/2 < z < (h_s - h_f)/2 \\ \varepsilon_s & (h_s - h_f)/2 < z < h/2 \end{cases} \tag{A6}$$

where the plate thickness *h* is divided into 'substrate' and 'film' regions of thickness h_s, h_f respectively, ε_s is the thermal strain in the substrate and ε_m is an additional, or mismatch, strain in the film.

The laminate stiffness and driving moments are,

$$A_{ij} = Q_{ij} h \quad B_{ij} = 0 \quad D_{ij} = Q_{ij} h^3/12$$
$$M^t = (Q_{11} + Q_{12}) \frac{\varepsilon_d h_f h_s}{2} \tag{A7}$$

The H coefficients and λ are then,

$$H_1^* = Q^3{}_{11} \nu (1-\nu^2)/12$$
$$H_2^{\varepsilon} = Q^3{}_{11} (1-\nu)(1+\nu)^2 \frac{\varepsilon_m h_f h_s}{2h^2}$$
$$H_4^* = Q^3{}_{11} (1-\nu^2)/12 \tag{A8}$$
$$H_3^* = Q^3{}_{11} \frac{\phi(1-\nu^2)^2}{768(4 + (1-\phi)(\nu-3))}$$
$$\lambda = \frac{\phi - 1}{24} Q^3{}_{11} (1+\nu)(1-\nu)^2$$

so that, after substitution into () the mismatch strains required for parallel or diagonal bifurcation are,

$$\varepsilon_m^p = \frac{4}{3(1+\nu)^{3/2}} \left(\frac{h}{R}\right)^2 \left(\frac{h^2}{h_f h_s}\right) \sqrt{\frac{1 + (\phi - 1)(3-\nu)/4}{\phi}} \tag{A9}$$
$$\varepsilon_m^d = \varepsilon_m^p \sqrt{\phi}\,(1 - (1-\nu)(1-\phi)/2)$$

for $\phi = 1$ both are equal, and in the thin film limit, $h \to h_s$ so that the critical strain is,

$$\varepsilon_m^p = \varepsilon_m^d = \frac{4}{3(1+\nu)^{3/2}} \left(\frac{h_s}{R}\right)^2 \frac{h_s}{h_f} \tag{A10}$$

which agrees exactly with Freund's prediction found by combining Eq (10) and Eq (5) in that paper.

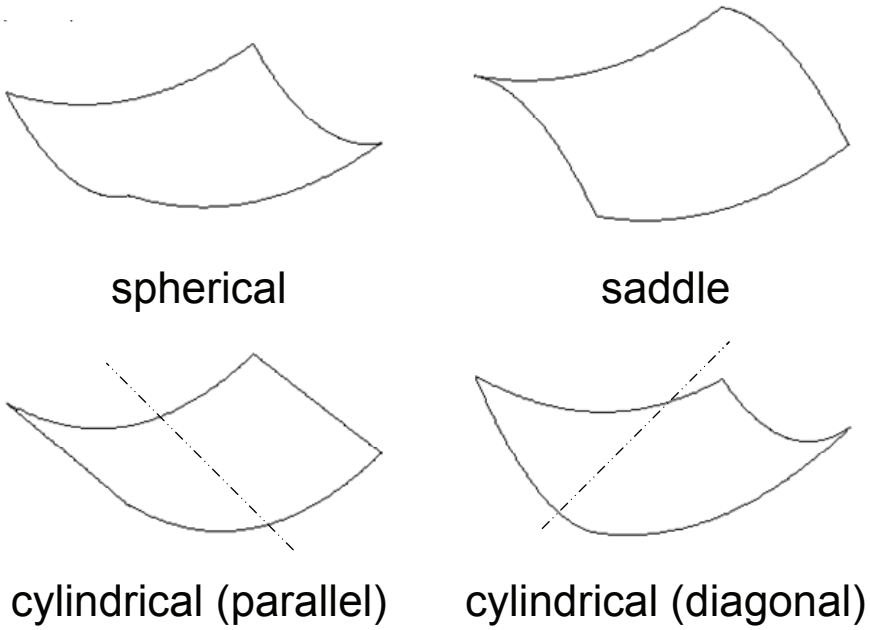

Figure 1. a) Schematic of deformation shapes. The spherical shape is observed for small strain for the square-symmetry case. Saddle modes are observed for orthogonal cross-ply laminates. The edge-parallel and diagonal cylindrical shapes are observed for large strain in the square symmetry case..

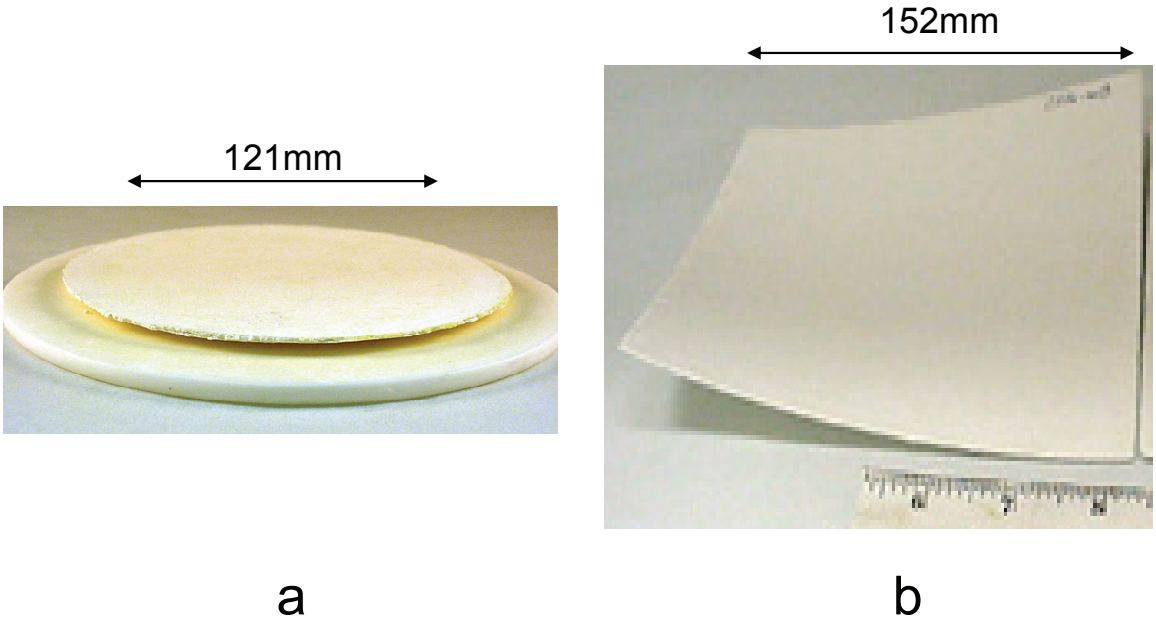

Figure 2 Mixed fiber CMC places exhibiting different bifurcation modes a) 120 mm circular plate shows symmetric deformation b) 150 mm square plate shows diagonal deformation.

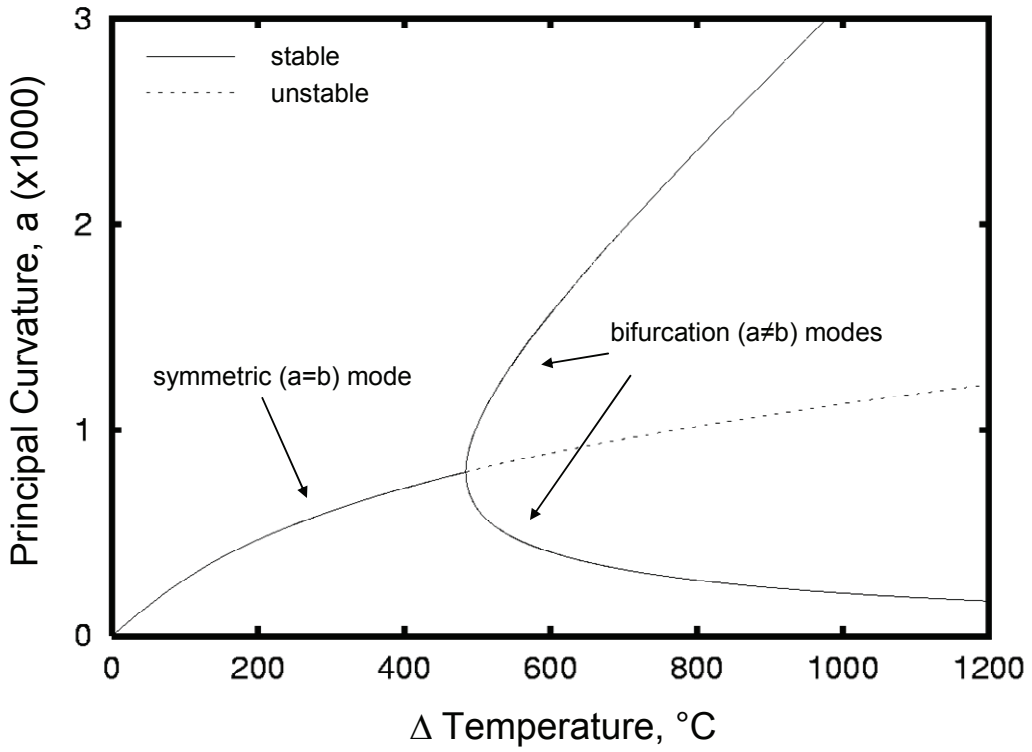

Figure 3. Isotropic plate deformation. A 1.25 mm thick by 150mm square plate with properties given by Eq (17) and (17a) with $\phi = 1$.

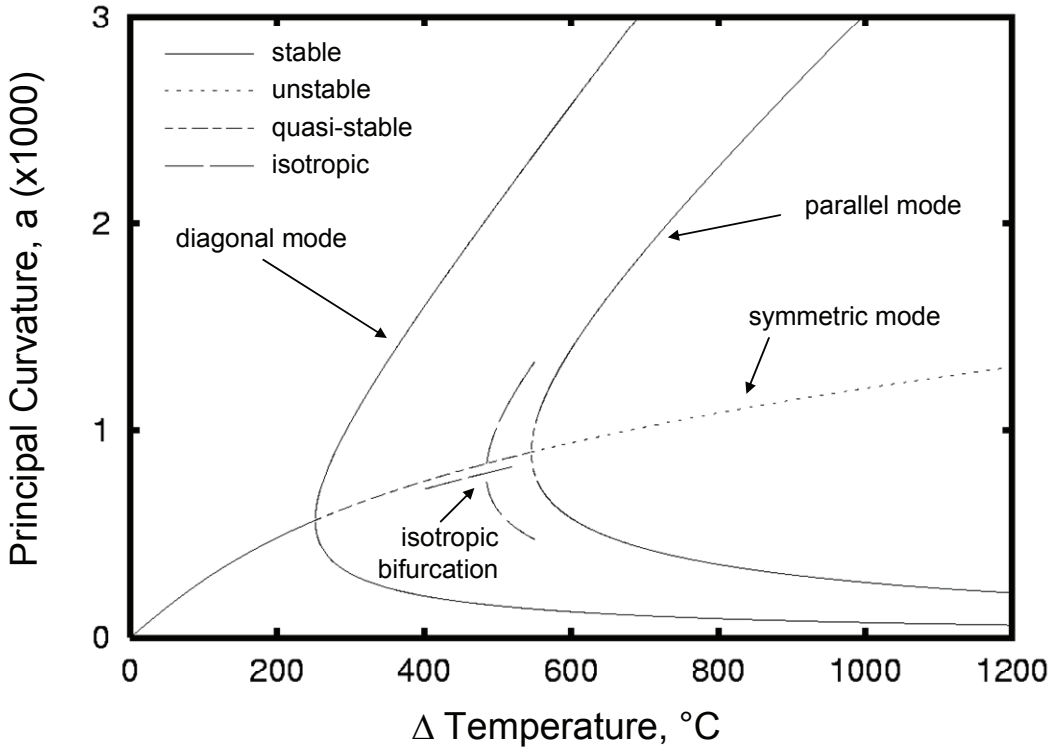

Figure 4. Reduced shear plate deformation.

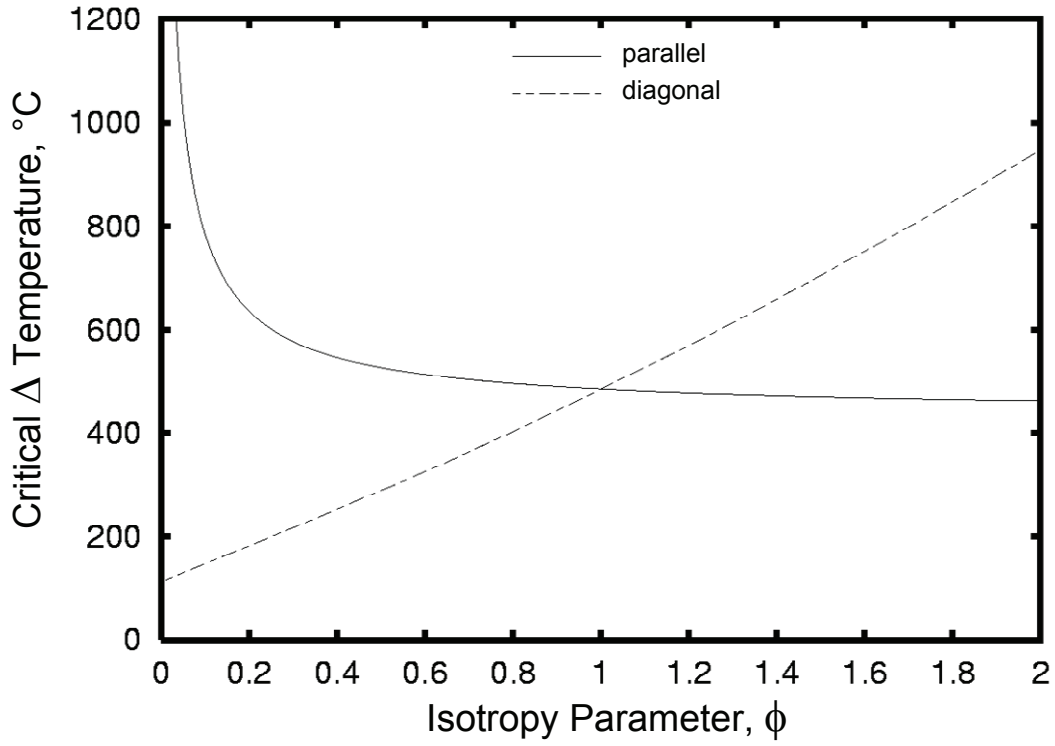

Figure 5 Critical temperature vs ϕ

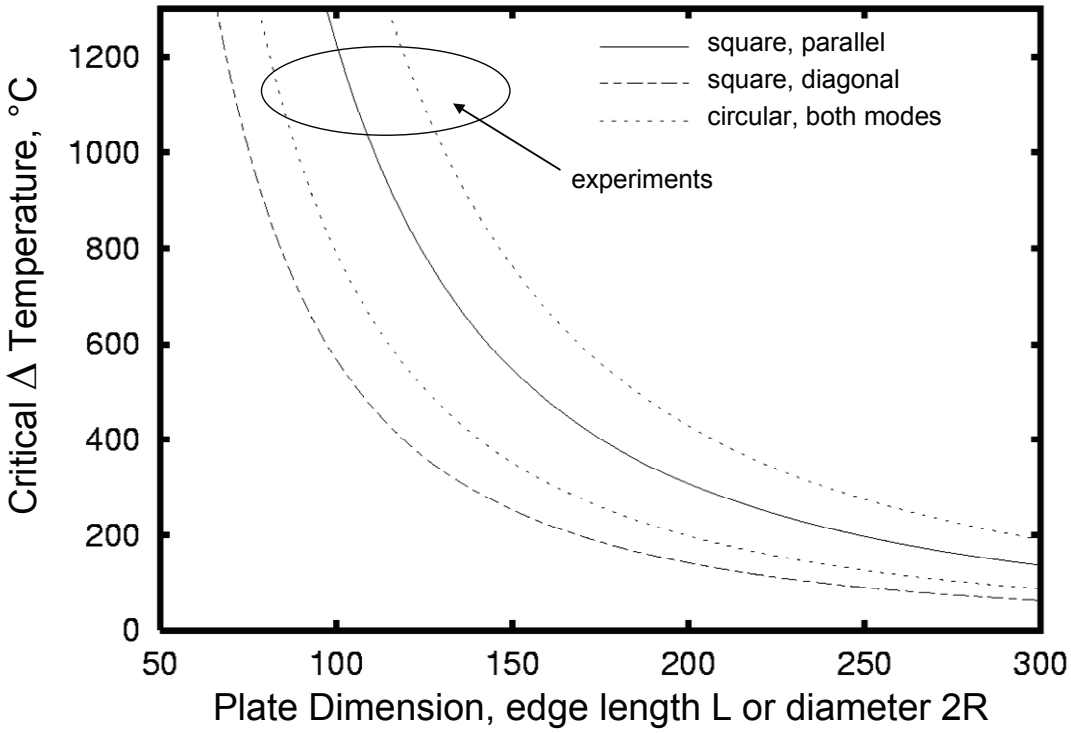

Figure 6 critical temp vs. plate size.

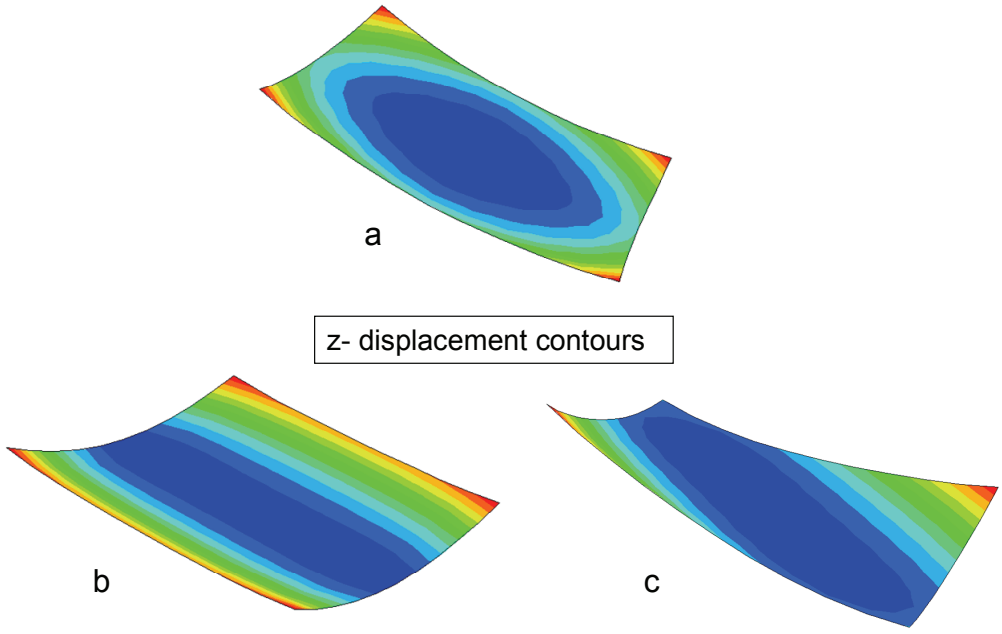

Figure 7. Finite element simulation. a) primary solution b) edge-parallel mode c) diagonal mode

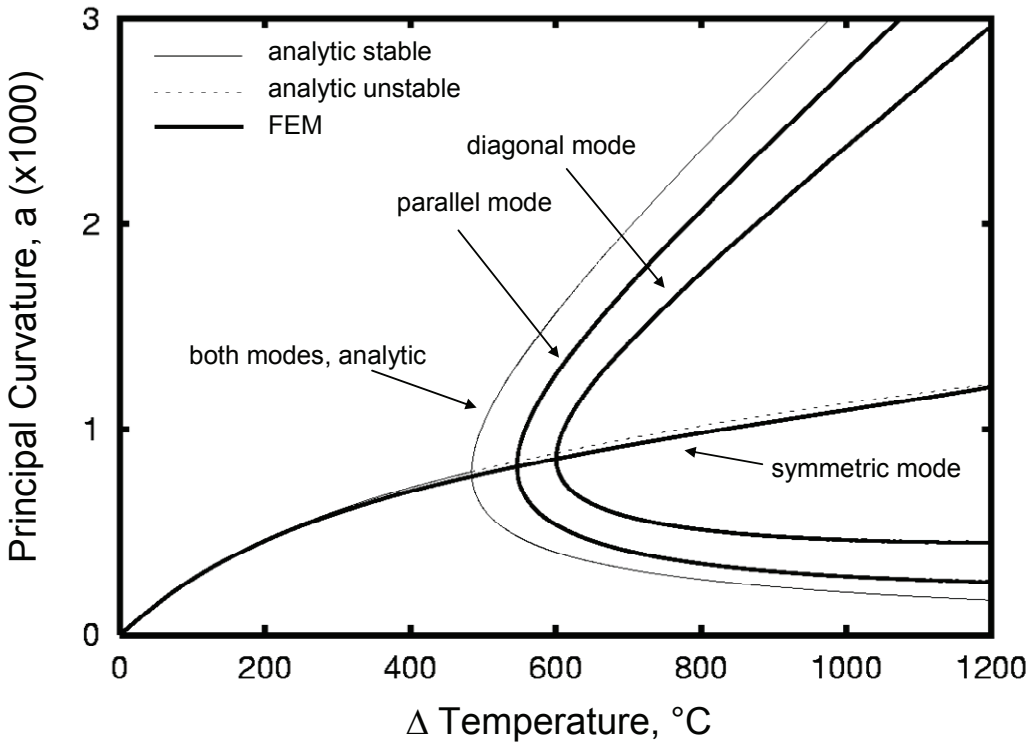

Figure 8. Finite element simulation results for an isotropic plate.

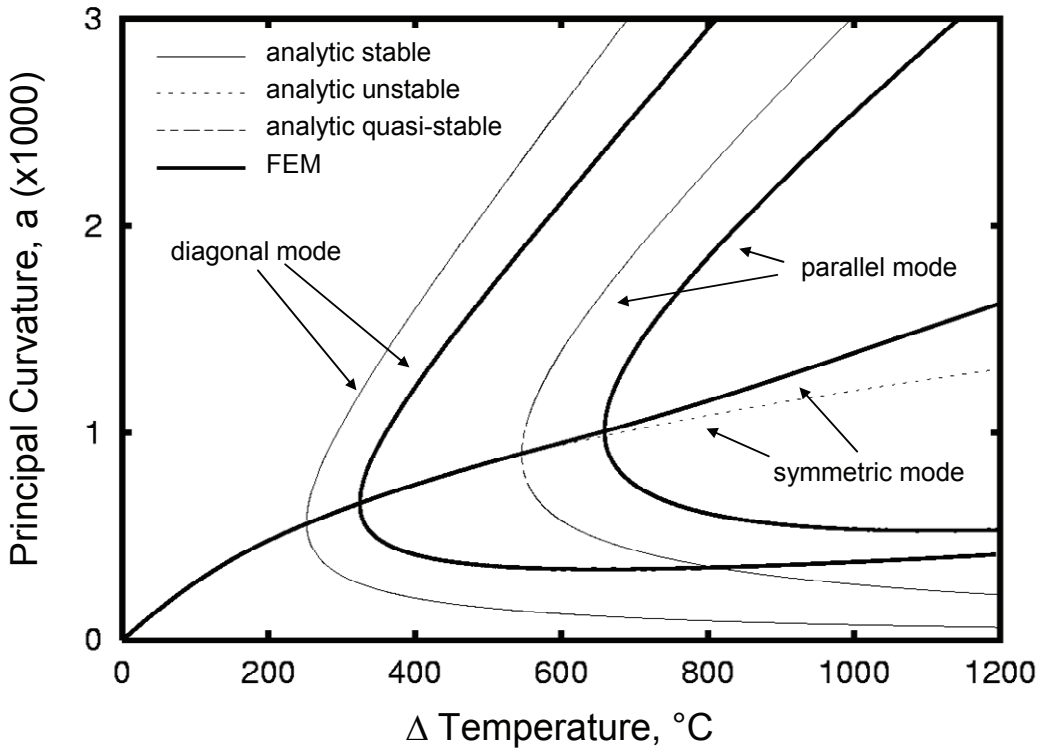

Figure 9. Finite element simulation results for ϕ=0.4.

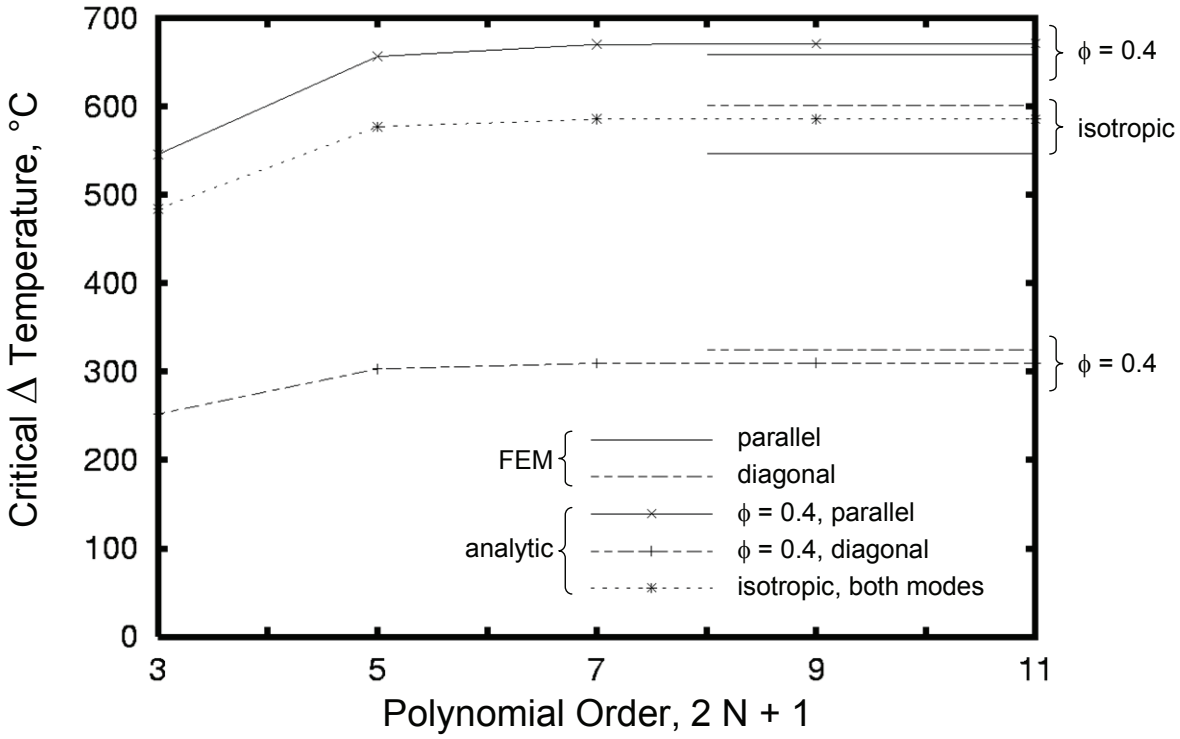

Figure 10 Convergence of high-order solutions.